The electrochemical reduction of dioxygen and hydrogen peroxide by molecular copper catalysts

Langerman, M.

Chapter 2

Fast oxygen reduction catalysed by a copper(II) tris(2-pyridylmethyl)amine complex via a stepwise mechanism

Catalytic pathways for the reduction of dioxygen can either lead to the formation of water or peroxide as the reaction product. We demonstrate that the electrocatalytic reduction of O_2 by the pyridylalkylamine copper complex $[Cu(tmpa)(L)]^{2+}$ in neutral aqueous solution follows a stepwise $4e^-/4H^+$ pathway, in which H_2O_2 is formed as a detectable intermediate and subsequently reduced to H_2O in a separate catalytic reaction. These homogeneous catalytic reactions are shown to be first order in catalyst. Coordination of O_2 to Cu^I is found to be the rate determining step in the formation of the peroxide intermediate. Furthermore, the electrochemical study of the reaction kinetics reveals a high turnover frequency of 1.5×10^5 s^{-1}, the highest reported for any molecular copper catalyst.

Adapted from M. Langerman, D. G. H. Hetterscheid, *Angew. Chem. Int. Ed.* **2019**, *58*, 12974-12978.

2.1. Introduction

With the shift in the energy landscape from fossil fuels towards sustainable sources of energy, storage and conversion of fuels such as hydrogen is expected to play an important role. It is therefore important that efficient fuel cells are available to minimize energy loss during fuel-to-energy interconversion. However, the cathodic oxygen reduction reaction (ORR) is a significant limiting factor in the efficiency of fuel cells.[1-2] In nature, multicopper oxidases such as laccase are known to catalyse the four-electron reduction of O_2 to H_2O efficiently.[3] Immobilization of Laccase on electrodes has shown that the ORR can be performed close to the thermodynamic equilibrium potential of water.[4-9] In the effort to create synthetic mimics of these copper enzymes, a wide range of model copper systems have been studied for their oxygen activation reactivity.[9-13] While some early examples of copper complexes have been studied for their activity towards the ORR,[14-18] only in the last decade have the first molecular copper model catalysts been evaluated for their ORR activity, either by means of sacrificial reductants or via electrochemical studies.[19-24] $[Cu(tmpa)(L)]^{2+}$ (tmpa = tris(2-pyridylmethyl)amine), L = solvent) and many derivatives of the pyridylalkylamine template have been studied as a mimic for active sites in redox active metalloenzymes for its non-planar and flexible coordination sphere and its reactivity towards dioxygen.[13, 25-27] The dioxygen binding chemistry of Cu-tmpa has been thoroughly studied by Karlin *et al.*[28-30] It was shown that in a range of solvents, the binding of dioxygen to $[Cu^{I}(tmpa)]^{+}$ leads to fast formation of an end-on Cu^{II} superoxo complex, followed by a slower dimerization step to form a dinuclear copper peroxo complex. Additionally, Fukuzumi and Karlin have studied the ORR activity of Cu-tmpa in acetone, using decamethylferrocene as a sacrificial reductant, which involves a dinuclear intermediate.[19, 22] Recently, it was shown that heterogenized Cu-tmpa, and several derivatives, adsorbed on carbon black catalyse the electrochemical ORR in aqueous buffer solutions.[21, 31] Additionally, the electrochemical ORR activity of homogenous Cu-tmpa dissolved in aqueous solution has been investigated, as well as pH effects on the redox chemistry.[32-33] However, thus far catalytic rates have not been reported and the mechanism wherein ORR occurs has not been elucidated.

The field of homogeneous electrocatalysis for the conversion of small molecules (O_2, CO_2, H_2O, H_2, *etc.*) is expanding rapidly, and great strides have been made to develop new methods to be able to study their reaction kinetics and to allow for benchmarking of different catalysts.[34-37] Foot-of-the-wave analysis (FOWA) has become an important tool to determine the catalytic performance of homogeneous electrocatalysts, as it allows for the determination of rate constants under limiting conditions.[34, 37-42] Using these methods, we have quantified the fast electrocatalytic ORR by homogeneous Cu-tmpa in neutral aqueous solution. Additionally, a comprehensive study of the product

formation using R(R)DE techniques has provided important new insight into the electrocatalytic ORR mechanism, and shows that catalysis occurs via a stepwise mechanism at a single copper centre.

2.2. Results and Discussion

The redox and catalytic behaviour of Cu-tmpa in a phosphate buffer (PB) solution at pH 7, containing 100 mM phosphate salts (NaH_2PO_4 and Na_2HPO_4), was investigated. Cyclic voltammograms (CVs) of Cu-tmpa were recorded using a Glassy Carbon (GC) working electrode (A = 0.0707 cm^2). In the presence of 1 atm argon, a well-defined reversible Cu^{I}/Cu^{II} redox couple is visible at $E_{1/2}$ = 0.21 V vs. RHE, shown in Figure 2.1. In the presence of 1 atm O_2, a peak-shaped catalytic wave appears with an onset potential at 0.5 V vs. RHE. This peak-shaped catalytic wave is characteristic for cases of substrate depletion, demonstrating the fast catalysis by Cu-tmpa. The homogeneity of the catalyst was established by electrochemical quartz crystal microbalance (EQCM) experiments, both under non-catalytic and catalytic conditions (Appendix A.2).[43-46]

Determination of the relationship between the catalytic current and the catalyst concentration would provide useful insight towards the possible mechanism for the ORR. Due to the low solubility of O_2 in most solvents, aqueous or otherwise, either very high O_2 pressures or low catalyst concentrations must be used to avoid the O_2 mass-transport limitation. By measuring CVs in the presence of 1 atm O_2 at low catalyst concentrations (0.1–1.0 µM Cu-tmpa), a linear first-order dependence of the catalytic current on the catalyst concentration was observed (Figure A.5).

To determine product selectivity and the electron-transfer number of the catalyst in neutral aqueous solution, rotating (ring-)disk electrode (R(R)DE) voltammetry was used. Previous hydrodynamic studies on the electrocatalytic ORR performance of Cu-tmpa have been carried out using a Vulcan supported surface deposit of Cu-tmpa[21, 31], or only evaluated the behaviour of Cu-tmpa in aqueous solution under non-catalytic conditions.[33] While R(R)DE voltammetry is most often used to study heterogeneous catalytic reactions, it can be used to study homogeneous catalytic reactions under certain conditions. One of the main difficulties with the use of the R(R)DE methods for homogeneous catalysts is that both the product and substrate are present in the liquid phase. For complex multi-electron multi-step catalytic reactions (ECE, or ECEC') such as the ORR, this can result in significant deviations from the behaviour dictated by the Koutecky-Levich (KL) equation, which governs the behaviour of reactions with one diffusing species. In such cases, slow catalysis will result in non-ideal behaviour of the measured limiting currents as a function of the rotation rate, and deviations from linearity will be observed in KL-plots. However, for fast catalytic reactions, the limiting current corresponds to the electron transfer number (n) of the catalytic reaction.[47] In

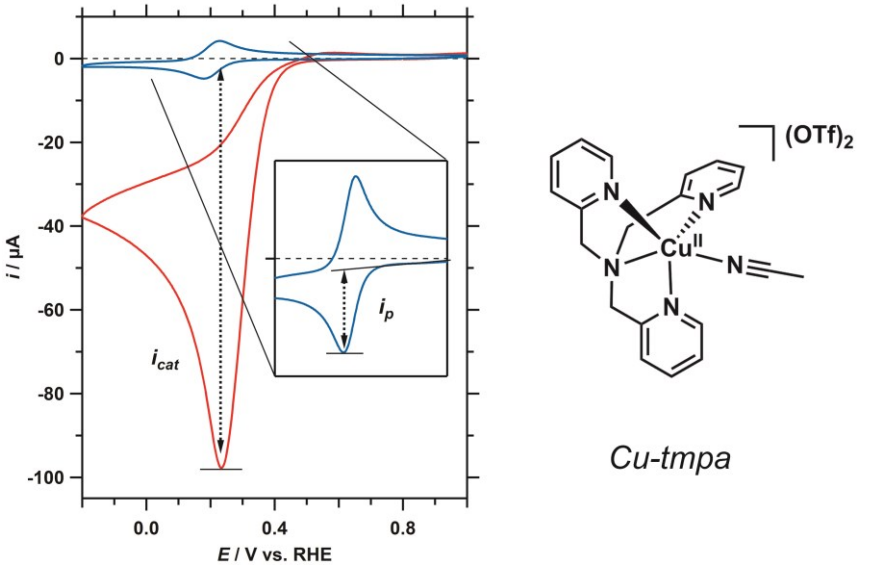

Figure 2.1. CVs of Cu-tmpa (0.32 mM) in the presence of 1 atm Ar (blue, zoom in inset) or 1 atm O_2 (red). $E_{cat/2}$ = 0.31 V vs. RHE. Conditions: pH 7 PB ([PO_4] = 100 mM), 1 atm O_2, 293 K, 100 mV s^{-1} scan rate.

effect, sufficiently fast molecular catalysts (where *k* >> rotation rate) can be considered to behave as heterogeneous within this time frame. Indeed, this is exactly what is observed in the case of Cu-tmpa. Figure 2.2a shows a clear positive shift in the ORR onset potential to 0.5 V vs. RHE in the presence of Cu-tmpa compared to the bare GC electrode. KL analysis was performed on the mass-transport limiting current (I_L) obtained at different rotation rates (Figure 2.2b/c). Indeed, good linearity is achieved in the KL-plot, similar to that of a Pt disk electrode. This shows that *n* is constant as a function of rotation rate under these conditions. The number of electrons involved in the homogeneous ORR catalysed by Cu-tmpa was determined to be 3.9 (see Appendix A.5), which shows the high selectivity towards the 4-electron reduction of dioxygen. This selectivity is in agreement with the heterogenized carbon black supported Cu-tmpa system.[21]

For product determination on the Pt ring electrode, it is important to account for any contributions from reduced catalytic intermediate species towards the observed ring current, as these species could also be oxidized at the ring. A small oxidative ring current can be seen from 0.5 to 0.1 V vs RHE during catalysis, which decreases as the mass-transport limited current is reached (Figure 2.2a, red trace). The observed ring current during the ORR in the presence of Cu-tmpa is negligible when compared to the GC electrode, which itself is well-known to catalyse the 2-electron reduction of O_2 to H_2O_2. To exclude the possibility that the observed ring current during ORR is caused by

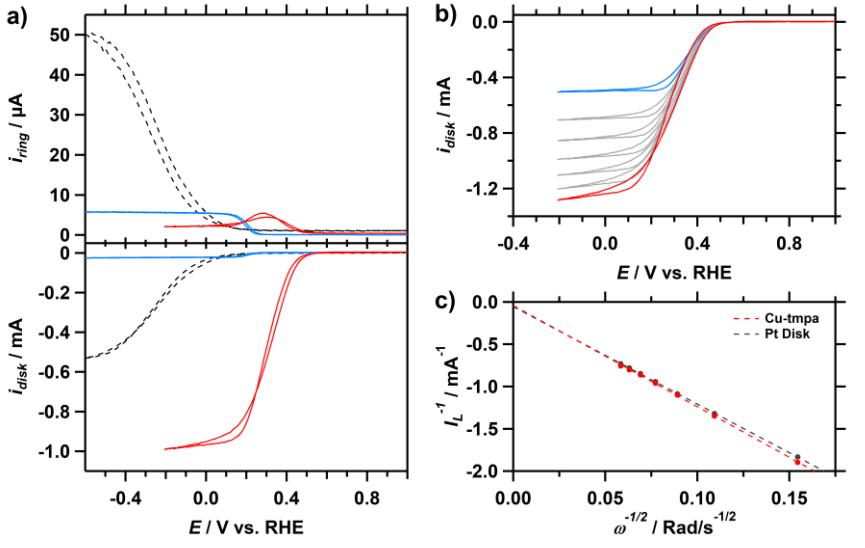

Figure 2.2. a) RRDE CVs of bare GC (dotted line) under 1 atm O_2 and Cu-tmpa (0.3 mM) under 1 atm Ar (blue) and 1 atm O_2 (red) at 1600 RPM. **b)** Disk current of Cu-tmpa (0.3 mM) under 1 atm O_2 at different rotation rates from 400 RPM (blue line) to 2800 RPM (red line); 400 RPM increments. **c)** Koutecky-Levich plot of the inverse limiting current (I_L^{-1}) at –0.2 V (vs. RHE.) as a function of the inverse square root of the rotation rate. Conditions: pH 7 PB ([PO_4] = 100 mM), 293 K, Pt ring at 1.2 V vs. RHE, 50 mV s^{-1} scan rate.

the oxidation of a (partially) reduced catalytic species, the fixed potential applied to the Pt ring was set below the onset potential of H_2O_2 oxidation on Pt. Decreasing the fixed potential on the ring from 1.2 to 0.8 V vs. RHE, which is still higher than the Cu^{I}/Cu^{II} redox couple, eliminated the oxidation event taking place on the Pt ring (Figure A.8b). This potential dependence indicates that the observed ring current is due to oxidation of H_2O_2. In addition, the ring current actually significantly increases upon a 300 times decrease in catalyst concentration (Figure A.9). This increase would not be possible if the species that is oxidized by Pt would be a Cu_x-O_2 intermediate. This shows that the oxidative event on the ring can be attributed to H_2O_2 oxidation.

Quantification of the percentage H_2O_2 (%H_2O_2) produced during ORR was achieved using Eq. 2.1, using the disk current (i_{disk}), ring current (i_{ring}), and the collection efficiency of H_2O_2 of the Pt ring (N_{H2O2}). %H_2O_2 was determined from chronoamperometric measurements at a range of potentials below 0.5 V vs. RHE for Cu-tmpa concentrations of 0.3 mM and 1.0 µM (Appendix A.7). At the onset of the catalytic activity, significant amounts of H_2O_2 are detected, both for catalyst concentrations of 0.3 mM (ca. 75%) and 1.0 µM (ca. 90%) (Figure 2.3). A plateau of %H_2O_2 is clearly visible at the catalytic onset at the lower concentration, while this is less pronounced at higher catalyst concentration. These percentages decrease with decreasing potential and upon

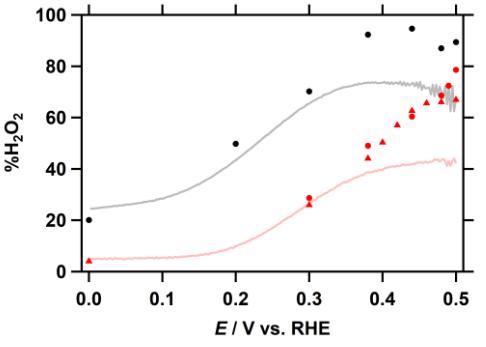

Figure 2.3. $\%H_2O_2$ obtained from RRDE CA (dots and triangles) and LSV (lines, 50 mV s^{-1}) measurements as a function of applied potential at a rotation rate of 1600 RPM with 0.3 mM (red), and 1.0 µM (black) Cu-tmpa. Conditions: pH 7 PB ($[PO_4]$ = 100 mM), 293 K, Pt ring at 1.2 V vs. RHE.

reaching the limiting current potential regime the $\%H_2O_2$ stabilizes at 4% and 20% at 0.0 V vs. RHE for 0.3 mM and 1.0 µM Cu-tmpa, respectively. However, below 0.1 V a contribution of the GC electrode towards H_2O_2 production cannot be excluded. These results show that a catalytic reaction that leads to the formation H_2O_2 is active over the entire catalytic potential window.

$$\%H_2O_2 = \frac{2 \times (i_{ring}/N_{H2O2})}{i_{disk} + (i_{ring}/N_{H2O2})} \times 100 \qquad (2.1)$$

Conversion of i_{disk} measured during RDE experiments to the kinetic current density (j_k) allows for the evaluation of Tafel slopes of the ORR in the potential region where the current is not mass-transport limited. By plotting the applied potential as a function of the logarithm of j_k a Tafel plot can be constructed (Figure 2.4). As we are dealing with a homogeneous multi-electron, multistep catalytic reaction with several diffusing species, care should be taken not to over-interpret the Tafel slopes, or derive specific $e^-(/H^+)$ transfer steps from the Tafel slope values. In the presence of O_2, a clear change of Tafel slope from is seen around 0.38 V vs. RHE, while in the presence of H_2O_2 under the exact same conditions no change in slope is observed. The observed slope change during ORR indicates that a different process becomes rate-determining. The potential at which this occurs closely matches the potential where half the limiting current is observed and is below the onset potential (ca. 0.45 V) of H_2O_2 reduction by Cu-tmpa (Figure A.14). The Tafel slope observed for the reduction of H_2O_2 by Cu-tmpa is very similar to the −136 mV/dec slope between 0.38 V and 0.20 V during the ORR, which indicates that the same step in the mechanism is rate-determining in this regime. Tafel slopes derived from measurements performed at low (1.0 µM) catalyst concentration show the same behaviour as at higher Cu-tmpa concentration (Figure A.15).

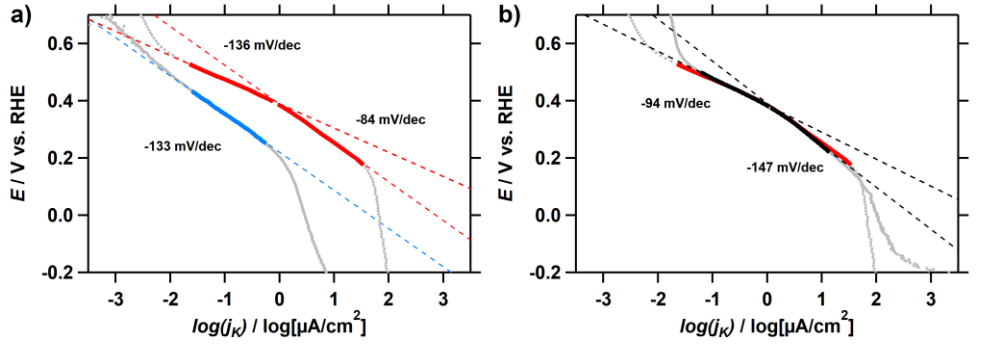

Figure 2.4. a) Plot of Tafel slopes derived from RRDE CV at 1600 RPM in the presence of 0.3 mM Cu-tmpa and 1 atm O_2 (red lines) or 1.1 mM H_2O_2 (blue line). **b)** Tafel slopes in the presence of 0.3 mM (red lines) and 1.0 μM (black lines) Cu-tmpa under 1 atm O_2. Conditions: pH 7 PB ([PO_4] = 100 mM), 293 K, 50 mV s^{-1} scan rate.

Turnover frequencies (TOFs, s^{-1}) were obtained from electrochemical measurements; either by direct determination using the catalytic current enhancement,[35] or by applying the foot-of-the-wave analysis (FOWA).[34, 37-39] At the onset of the catalytic wave the catalytic reaction is assumed to be under kinetic conditions. As such, FOWA is not affected by side phenomena such as substrate consumption, catalyst deactivation, or product inhibition. It is therefore especially useful for the ORR, where substrate consumption plays an important role. If more reliable kinetic conditions can be achieved during catalysis, the observed first order rate constant k_{obs} (or TOF) for the ORR can be directly determined from the catalytic current enhancement (i_{cat}/i_p) by applying Eq. 2.2.

$$\frac{i_{cat}}{i_p} = 2.24n\sqrt{\frac{RT}{Fv}k_{obs}} \qquad (2.2)$$

Here i_{cat} and i_p refer to the maximum catalytic current and the peak reductive current of the $Cu^{(II/I)}$ redox couple, respectively (Figure 2.1).[35] From the current enhancement derived at low catalyst concentration (0.1–1.0 μM), a TOF of $1.5\times10^5 \pm 0.2\times10^5$ s^{-1} was obtained (Appendix A.9, Figure A.15). It is important to note that this TOF is associated with the overall 4e catalytic reaction. However, as shown by the RRDE measurements and Tafel slope analysis, there are two different rate-determining catalytic regimes. Interestingly, FOWA can be employed to determine the k_{obs} (or TOF_{max}) associated with the partial reduction of O_2 to H_2O_2, as FOWA only uses the foot of the catalytic wave where H_2O_2 reduction rates are still negligible. The TOF_{max} for Cu-tmpa in pH 7 phosphate buffer in the presence of 1 atm O_2 was found to be $1.8\times10^6 \pm 0.6\times10^6$ s^{-1}.

It has been firmly established by stopped-flow experiments that oxygen binding to $[Cu^{I}(tmpa)]^{+}$ proceeds via a fast equilibrium to initially produce $[Cu^{II}(O_2^{\bullet-})(tmpa)]^{+}$ as a detectable intermediate.[29] This species subsequently forms the $[\{Cu^{II}(tmpa)\}_2(\mu\text{-}O_2)]^{2+}$ dimer in a reaction that is consistently slower than the initial oxygen binding over a wide temperature and solvent range. If catalysis were to proceed via such a dimeric species, it should lead to a second order dependence in Cu-tmpa. Instead, the observed linearity in the FOWA region is in agreement with a catalytic first order relationship in catalyst (see Appendix A.9),[38] and is in good agreement with the first order catalyst concentration dependence discussed previously. That catalysis can indeed occur at a single site copper species was demonstrated previously using a site isolated immobilized copper phenanthroline system, albeit with a very low catalytic conversion to H_2O_2.[20]

The TOF_{max} associated with the first $2e^-/ 2H^+$ reduction step to H_2O_2 is the same, within the error margin, as the TOFs (also determined by FOWA) of the fastest iron porphyrin complexes (2.2×10^6 s^{-1}) recently reported by Mayer *et al.*, which are the fastest homogeneous ORR catalysts in acetonitrile reported to date.[23, 48] When accounting for the oxygen solubility difference using $TOF = k_{O2}[O_2]$, where $[O_2] \approx 1.1$ mM in water ($[PO_4]$= 100 mM) under 1 atm O_2, the obtained second-order rate constant k_{O2} = 1.6×10^9 ($\pm$ 0.5×10^9) M^{-1} s^{-1} is an order of magnitude faster than the aforementioned iron porphyrins. This k_{O2} is comparable to the second order rate constant of O_2 binding, k_{O2} = 1.3×10^9 M^{-1} s^{-1}, found for Cu^{I}-tmpa in THF, which represents the fastest k_{O2} among copper complexes and hemes; both synthetic and natural.[30]

The $\%H_2O_2$ quantification and analysis of Tafel slopes derived from RRDE measurements provide a strong indication that the ORR goes through a stepwise mechanism (see Scheme 2.1). Herein O_2 is first reduced to H_2O_2, which in turn is further reduced to H_2O upon reaching the required potential. In this case the overall reaction will still yield a catalytic electron transfer number close to 4 in the O_2 mass-transport limited regime, as was established by KL and RRDE analysis. The onset potential of H_2O_2 reduction by Cu-tmpa is around 0.45 V vs. RHE, roughly 50 mV lower than that of O_2 reduction. The difference between onset potentials is small, which explains why $\%H_2O_2$ quickly lowers upon decreasing the potential. At low catalyst concentration a catalyst diffusion effect is observed and $\%H_2O_2$ is stable over a larger potential range before decreasing. This is expected as oxygen is a competitive inhibitor of H_2O_2 reduction. Peroxide will accumulate more at low catalyst concentrations, whereas it is more rapidly reduced at higher catalyst loadings while maintaining the same amounts of oxygen in solution. As both the ORR Tafel slope below 0.38 V and the Tafel slope for H_2O_2 reduction by Cu-tmpa are the same, it gives a strong indication the reduction of

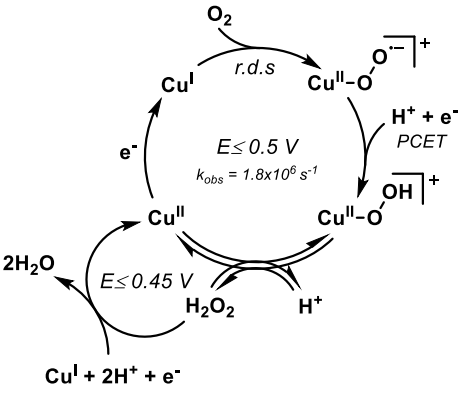

Scheme 2.1. Proposed stepwise mechanism for the electrocatalytic ORR by Cu–tmpa in neutral aqueous solution. For clarity, the tmpa ligand is not depicted. PCET = proton-coupled electron transfer.

H_2O_2 to H_2O is rate determining in this potential window during the ORR. When FOWA is applied to determine the rate constant of the partial reduction of O_2 to H_2O_2, linearity of the catalytic current is only observed when applying the FOWA expression corresponding to a first order catalytic system (see Appendix A.9). This shows that the partial reduction of O_2 to H_2O_2 is also first order in catalyst. The initial quantitative accumulation of hydrogen peroxide, the kink in the Tafel slope and its independence on the Cu-tmpa concentration, and the first order rate dependence in Cu-tmpa throughout point to two separate catalytic cycles, wherein H_2O_2 is readily replaced in the coordination sphere of copper (see Scheme 2.1).

2.3. Conclusion

Our findings contrast the previously proposed dinuclear mechanism for the ORR by Cu-tmpa using sacrificial reductants in acetone, where fast O_2 binding resulting in a copper superoxo species was followed by a slower dimerization step.[19] Under aqueous electrochemical conditions, fast electron transfer and high proton mobility resulting in a fast PCET step most likely favours the formation of the hydroperoxo complex over dimerization.

To conclude, the electrocatalytic ORR activity of Cu-tmpa in neutral aqueous solution was quantified, revealing very fast kinetics and high TOFs. The rate constants reported here are the first rate constants reported for the electrochemical reduction of O_2 by a homogeneous copper complex. Application of the FOWA revealed that the TOF associated with the partial reduction of O_2 is very close to the O_2 binding constant with Cu-tmpa. This suggests that coordination of dioxygen to Cu^I is the rate determining step in the formation of peroxide. Additionally, we have shown that in aqueous solution the

ORR occurs at a single Cu-tmpa centre through a stepwise type mechanism, in which O_2 first undergoes 2-electron reduction to H_2O_2, followed by 2-electron reduction of H_2O_2 to H_2O. This stepwise mechanism was first mentioned as one of the possible mechanisms for Cu-tmpa by Asahi *et al.*, based on the ability of Cu-tmpa to catalyse the H_2O_2 reduction.[32] However, until now there has been no direct evidence on whether a stepwise reaction actually takes place during ORR. This work provides new insight the oxygen reduction reaction mediated by copper, and opens new possibilities towards the electrochemical synthesis of hydrogen peroxide relevant to energy conversion reactions, given that peroxide is an excellent candidate as a renewable fuel.

2.4. Experimental

2.4.1. General

Di-(2-picolyl)amine, 2-pyridinecarboxaldehyde, and sodium triacetoxyborohydride were obtained from Sigma Aldrich. $Cu(OTf)_2$ was obtained from Alfa Aesar. THF and CH_3CN were obtained from Sigma-Aldrich and dried using a PureSolve 400 solvent dispenser. Filtration and isolation of the complex was done using Whatman® RC60 membrane filters. Aqueous electrolyte solutions were prepared using NaH_2PO_4 (Suprapur®, Merck), Na_2HPO_4 (Suprapur®, Merck), Na_2SO_4 (Suprapur®, Merck), and NaOH (TraceSelect ≥ 99.9995%, Fluka). Elemental analysis was performed by Mikroanalytisches Laboratorium Kolbe. Milli-Q Ultrapure grade water was used for all electrochemical experiments and for the preparation of all aqueous electrolyte solutions. Alumina suspensions (1.0, 0.3, and 0.05 µm) were obtained from Buehler. pH measurements were done using a Hanna Instruments HI 4222 pH meter which was calibrated using IUPAC standard buffers.

2.4.2. Synthesis

2.4.2.1. *Synthesis of tris(2-pyridylmethyl)amine – tmpa*

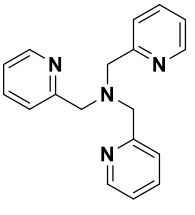

A modified literature procedure was used for the synthesis of tmpa.[49-50] Di-(2-picolyl)amine (4.0 mmol, 797 mg) and 2-pyridinecarboxaldehyde (4.0 mmol, 428 mg) were dissolved in dry THF (20 mL) under N_2 atmosphere. $NaBH(OAc)_3$ was added to the solution, followed by the addition of acetic acid (4.0 mmol, 0.229 mL). The reaction was stirred for 3 days at room temperature. The reaction was quenched with sat. $NaHCO_3$ (10 mL). The mixture was extracted with EtOAc and the organic layer was washed with sat. $NaHCO_3$ (10 mL). The solvent was removed by rotary, and the product was dissolved in $CHCl_3$. The solution was dried with $MgSO_4$ and filtered over a glass frit. Following removal of the solvent by rotary

evaporation, the product was obtained as off-white crystalline solid. Yield: 60% (2.40 mmol, 697 mg). ESI-MS: ^{1}H NMR (400 MHz, Methanol-d4) δ 8.43 (ddd, J = 5.0, 1.9, 0.9 Hz, 2H), 7.79 (td, J = 7.7, 1.8 Hz, 2H), 7.68 (dt, J = 7.9, 1.1 Hz, 2H), 7.27 (ddd, J = 7.6, 4.9, 1.3 Hz, 2H), 3.85 (s, 4H). ESI MS m/z (calc): 291.2 (291.2, $[M + H^+]^+$).

2.4.2.2. *Synthesis of [Cu(tmpa)(CH$_3$CN)](OTf)$_2$ – Cu-tmpa*

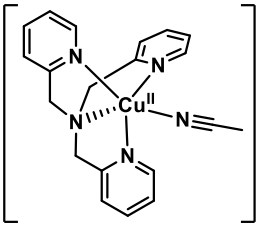

$Cu(OTf)_2$ (0.60 mmol, 218 mg) and tmpa (0.60 mmol, 173 mg) were dissolved in dry CH_3CN (20 mL) under N_2 atmosphere. A bright blue solution immediately formed, and the solution was allowed to stir for 1 hour. Et_2O (40 mL) was slowly added to the solution, and the complex was allowed to crystallize overnight at −18 °C. The crystals were filtered off and washed with Et_2O. After dissolving the crystals in CH_3CN, the crystallization step was repeated to obtain the complex as blue crystals. Yield: 69% (0.41 mmol, 285 mg). ESI MS m/z (calc): 502.1 (502.0, $[M - CH_3CN – OTf]^+$). Elemental analysis calcd (%) for $C_{20}H_{18}CuF_6N_4O_6S_2$ + 0.7 CH_3CN + 0.9 H_2O: C 36.88, H 3.17, N 9.45; found: C 37.09, H 3.42, N 9.24.

2.4.3. Electrochemical measurements

Autolab PGSTAT 12, 204, and 128N potentiostats in combination with Autolab NOVA software were used for all measurements. All electrochemical measurements apart from RRDE and EQCM experiments were performed in a custom-build glass 10 mL single-compartment cell with a three-electrode setup. All glassware used during the electrochemical measurements were regularly cleaned to remove impurities by overnight submersion in an aqueous 0.5 M H_2SO_4 solution containing 1 mg/mL $KMnO_4$, followed by removal of excess $KMnO_4$ from the glassware with diluted H_2SO_4 and H_2O_2. Finally, the glassware was subsequently rinsed five times and boiled two times in Milli-Q water. Prior to each experiment the glassware was boiled once in Milli-Q water. Glassy carbon (GC) was used as the working electrode and either a Teflon encapsulated GC rod (A = 0.0707 cm^2, type 1, Alfa Aesar), or a PEEK encapsulated GC (A = 0.0707 cm^2, Metrohm) were used in a submerged setup. Before every experiment the GC electrodes were manually polished with 1.0, 0.3, and 0.05 µm alumina suspensions on Buehler cloth polishing pads, for 5 minutes respectively, followed by sonication in Milli-Q water for 15 minutes. A gold wire was used as the counter electrode and was flame annealed and rinsed with Milli-Q water before each experiment. As a reference electrode a Pt mesh was used as the reversible hydrogen electrode (RHE) in the same buffer solution as the working electrode, connected via a Luggin capillary, and continuously sparged with H_2 gas. All gasses used during electrochemical measurements, H_2, O_2, and Argon

(5.0 grade), were supplied by Linde. Oxygen-free electrolyte solutions were prepared by sparging the cell for 30 minutes with argon, after which a 1 atm argon atmosphere was maintained. Oxygen-saturated electrolyte solutions were obtained by sparging the cell for 20 minutes with O_2, after which a 1 atm O_2 atmosphere was maintained.

2.5. References

[1] H. A. Gasteiger, S. S. Kocha, B. Sompalli, F. T. Wagner, *Appl. Catal. B* **2005**, *56*, 9-35.
[2] O. Gröger, H. A. Gasteiger, J.-P. Suchsland, *J. Electrochem. Soc.* **2015**, *162*, A2605-A2622.
[3] E. I. Solomon, U. M. Sundaram, T. E. Machonkin, *Chem. Rev.* **1996**, *96*, 2563-2606.
[4] V. Soukharev, N. Mano, A. Heller, *J. Am. Chem. Soc.* **2004**, *126*, 8368-8369.
[5] N. Mano, V. Soukharev, A. Heller, *J. Phys. Chem. B* **2006**, *110*, 11180-11187.
[6] C. F. Blanford, R. S. Heath, F. A. Armstrong, *Chem. Commun.* **2007**, 1710-1712.
[7] J. A. Cracknell, K. A. Vincent, F. A. Armstrong, *Chem. Rev.* **2008**, *108*, 2439-2461.
[8] C. F. Blanford, C. E. Foster, R. S. Heath, F. A. Armstrong, *Faraday Discuss.* **2009**, *140*, 319-335.
[9] C. E. Elwell, N. L. Gagnon, B. D. Neisen, D. Dhar, A. D. Spaeth, G. M. Yee, W. B. Tolman, *Chem. Rev.* **2017**, *117*, 2059-2107.
[10] E. A. Lewis, W. B. Tolman, *Chem. Rev.* **2004**, *104*, 1047-1076.
[11] J. Serrano-Plana, I. Garcia-Bosch, A. Company, M. Costas, *Acc. Chem. Res.* **2015**, *48*, 2397-2406.
[12] S. Hong, Y.-M. Lee, K. Ray, W. Nam, *Coord. Chem. Rev.* **2017**, *334*, 25-42.
[13] L. M. Mirica, X. Ottenwaelder, T. D. P. Stack, *Chem. Rev.* **2004**, *104*, 1013-1046.
[14] P. Vasudevan, Santosh, N. Mann, S. Tyagi, *Transit Met Chem* **1990**, *15*, 81-90.
[15] J. Zhang, F. C. Anson, *J. Electroanal. Chem.* **1992**, *341*, 323-341.
[16] J. Zhang, F. C. Anson, *J. Electroanal. Chem.* **1993**, *348*, 81-97.
[17] J. Zhang, F. C. Anson, *Electrochim. Acta* **1993**, *38*, 2423-2429.
[18] C. C. L. McCrory, X. Ottenwaelder, T. D. P. Stack, C. E. D. Chidsey, *J. Phys. Chem. A* **2007**, *111*, 12641-12650.
[19] S. Fukuzumi, H. Kotani, H. R. Lucas, K. Doi, T. Suenobu, R. L. Peterson, K. D. Karlin, *J. Am. Chem. Soc.* **2010**, *132*, 6874-6875.
[20] C. C. L. McCrory, A. Devadoss, X. Ottenwaelder, R. D. Lowe, T. D. P. Stack, C. E. D. Chidsey, *J. Am. Chem. Soc.* **2011**, *133*, 3696-3699.
[21] M. A. Thorseth, C. S. Letko, E. C. M. Tse, T. B. Rauchfuss, A. A. Gewirth, *Inorg. Chem.* **2013**, *52*, 628-634.
[22] S. Kakuda, R. L. Peterson, K. Ohkubo, K. D. Karlin, S. Fukuzumi, *J. Am. Chem. Soc.* **2013**, *135*, 6513-6522.
[23] M. L. Pegis, C. F. Wise, D. J. Martin, J. M. Mayer, *Chem. Rev.* **2018**, *118*, 2340-2391.
[24] S. Fukuzumi, Y.-M. Lee, W. Nam, *ChemCatChem* **2018**, *10*, 9-28.
[25] K. D. Karlin, J. C. Hayes, S. Juen, J. P. Hutchinson, J. Zubieta, *Inorg. Chem.* **1982**, *21*, 4106-4108.
[26] K. D. Karlin, S. Kaderli, A. D. Zuberbühler, *Acc. Chem. Res.* **1997**, *30*, 139-147.
[27] A. Wada, Y. Honda, S. Yamaguchi, S. Nagatomo, T. Kitagawa, K. Jitsukawa, H. Masuda, *Inorg. Chem.* **2004**, *43*, 5725-5735.
[28] K. D. Karlin, N. Wei, B. Jung, S. Kaderli, P. Niklaus, A. D. Zuberbuehler, *J. Am. Chem. Soc.* **1993**, *115*, 9506-9514.
[29] C. X. Zhang, S. Kaderli, M. Costas, E.-i. Kim, Y.-M. Neuhold, K. D. Karlin, A. D. Zuberbühler, *Inorg. Chem.* **2003**, *42*, 1807-1824.
[30] H. C. Fry, D. V. Scaltrito, K. D. Karlin, G. J. Meyer, *J. Am. Chem. Soc.* **2003**, *125*, 11866-11871.
[31] M. A. Thorseth, C. S. Letko, T. B. Rauchfuss, A. A. Gewirth, *Inorg. Chem.* **2011**, *50*, 6158-6162.
[32] M. Asahi, S.-i. Yamazaki, S. Itoh, T. Ioroi, *Dalton Trans.* **2014**, *43*, 10705-10709.
[33] M. Asahi, S.-i. Yamazaki, S. Itoh, T. Ioroi, *Electrochim. Acta* **2016**, *211*, 193-198.
[34] C. Costentin, S. Drouet, M. Robert, J.-M. Savéant, *J. Am. Chem. Soc.* **2012**, *134*, 11235-11242.
[35] R. M. Bullock, A. M. Appel, M. L. Helm, *Chem. Commun.* **2014**, *50*, 3125-3143.
[36] A. M. Appel, M. L. Helm, *ACS Catal.* **2014**, *4*, 630-633.
[37] E. S. Rountree, B. D. McCarthy, T. T. Eisenhart, J. L. Dempsey, *Inorg. Chem.* **2014**, *53*, 9983-10002.

[38] C. Costentin, J.-M. Savéant, *ChemElectroChem* **2014**, *1*, 1226-1236.
[39] D. J. Wasylenko, C. Rodríguez, M. L. Pegis, J. M. Mayer, *J. Am. Chem. Soc.* **2014**, *136*, 12544-12547.
[40] D. J. Martin, B. D. McCarthy, E. S. Rountree, J. L. Dempsey, *Dalton Trans.* **2016**, *45*, 9970-9976.
[41] C. Costentin, D. G. Nocera, C. N. Brodsky, *Proc. Natl. Acad. Sci.* **2017**, *114*, 11303-11308.
[42] C. Costentin, J.-M. Savéant, *J. Am. Chem. Soc.* **2017**, *139*, 8245-8250.
[43] N. D. Schley, J. D. Blakemore, N. K. Subbaiyan, C. D. Incarvito, F. D'Souza, R. H. Crabtree, G. W. Brudvig, *J. Am. Chem. Soc.* **2011**, *133*, 10473-10481.
[44] D. G. H. Hetterscheid, C. J. M. van der Ham, O. Diaz-Morales, M. W. G. M. Verhoeven, A. Longo, D. Banerjee, J. W. Niemantsverdriet, J. N. H. Reek, M. C. Feiters, *Phys. Chem. Chem. Phys.* **2016**, *18*, 10931-10940.
[45] D. G. H. Hetterscheid, *Chem. Commun.* **2017**, *53*, 10622-10631.
[46] B. van Dijk, J. P. Hofmann, D. G. H. Hetterscheid, *Phys. Chem. Chem. Phys.* **2018**, *20*, 19625-19634.
[47] P. A. Malachesky, L. S. Marcoux, R. N. Adams, *J. Phys. Chem.* **1966**, *70*, 4068-4070.
[48] M. L. Pegis, B. A. McKeown, N. Kumar, K. Lang, D. J. Wasylenko, X. P. Zhang, S. Raugei, J. M. Mayer, *ACS Cent. Sci.* **2016**, *2*, 850-856.
[49] J. Wang, C. Li, Q. Zhou, W. Wang, Y. Hou, B. Zhang, X. Wang, *Dalton Trans.* **2016**, *45*, 5439-5443.
[50] A. Podgoršek, M. Zupan, J. Iskra, *Angew. Chem. Int. Ed.* **2009**, *48*, 8424-8450.